49th AIAA Aerospace Sciences Meeting including the New Horizons Forum and Aerospace Exposition
4 - 7 January 2011, Orlando, Florida

AIAA 2011-383

E-CUSP Scheme for the Equations of Magnetothydrodynamics with High Order WENO Scheme

Yiqing Shen* Gecheng Zha†
Dept. of Mechanical and Aerospace Engineering
University of Miami
Coral Gables, Florida 33124
E-mail: yqshen@miami.edu, gzha@miami.edu

Manuel A. Huerta‡
Dept. of Physics, University of Miami
Coral Gables, Florida 33124

Abstract

An E-CUSP scheme is developed to solve the equations of magnetothydrodynamics. A fifth order WENO reconstructions are employed to calculate the fluxes in order to achieve high order spacial accuracy. Four standard testing cases, including two one-dimensional problems, the 2D Kelvin-Helmholtz instability and the Orszag-Tang MHD turbulence problem, are solved to validate the accuracy and robustness of the scheme. The 1D Brio-Wu shock tube problem is used to show the capability of capturing the compound waves in MHD. The other 1D problem tested is to demonstrate the robustness for high Mach number flow in MHD. The simulations of two 2D cases have demonstrated the capability of the new scheme to capture complex interactions of multiple shocks and vortices.

1 Introduction

The governing equations of magnetohydrodynamics(MHD) merge the hydrodynamics equations with Maxwell equations of electromagnetics. However, the electromagnetic field makes the structure of MHD equations more complex than that of hydrodynamics equations. There are seven eigenvalues and eigenvectors in the system of MHD equations, which means that there are seven different waves. In addition to the entropy wave, which propagates with the fluid speed, there are three other wave modes. According to the magnitude of the wave speeds, these three modes are called fast, intermediate(Alfven), and slow waves. The fast and slow waves are compressive, while the intermediate wave is not. Depending on the direction and the magnitude of the magnetic field, these wave speeds may coincide. Thus the MHD equations form a non-strictly hyperbolic system[1, 2, 3, 4, 5].

Since the ideal MHD equations have a wave-like structure analogous to that of the hydrodynamics equations, various numerical schemes for hydrodynamics equations have been extended to solve the MHD equations in the past two decades. The approximate Riemann solvers, which are based on eigenvalue and eigenvector analysis, are widely used for high speed flow as well as for high speed MHD applications. Beginning with the work of Brio and Wu[1], the numerical methods for MHD equations based on approximate

* Research Scientist, AIAA Member
† Associate Professor, AIAA Senior Member
‡ Professor

Riemann solvers have extensively been studied and developed. For example, Roe's Riemann solvers are developed by Brio and Wu[1], Dai and Woodward[6], Zachary and Collelaz[7], Roe and Balsara[2], and Cargo and Gallice[8]. HLL(Harten-Lax-van Leer)-type schemes are developed by Janhunen[9] and Honkkila and Janhunen[10], Gurski[11], Li[12], Miyoshi and Kusano[13], Balsara et al.[14]. Flux vector splitting methods are developed by MacCormack[15], Jiang and Wu[4]. The equations of magnetohydrodynamics are not homogeneous of degree one with respect to the state vector and hence can not directly perform flux vector splitting. To overcome this difficulty MacCormack introduces an extra variable $\tilde{a}$ in Ref. [15]. The flux splitting schemes based on eigenvalues and eigenvectors system are generally very complicated. In our study, we noticed that, in the eigensystem of Roe and Balsara[2], the eigenvalues of the Alfven waves have no affect on the flux. In other words, any values can be used for the eigenvalues of the Alfven waves and the flux will be the same. This makes the flux splitting based on Roe's approximate Riemann solver uncertain.

The low disspative high order filter schemes developed by Yee and Sjogreen[16] for MHD systems involves a dissipative portion of higher order Lax-Friedrichs scheme or an approximate Riemann solver. Moreover, Balbas[17] developed a central differencing scheme based on the evolution of cell averages over staggered grids. Gaitonde[18] developed a compact difference method for MHD with a local filter switching procedure to change the higher order filter to a second order filter locally for shock capturing. The central differencing scheme and the compact difference scheme do not need a detailed knowledge of the eigenstructure of the Jacobian matrices. However, the central differencing schemes have difficulty in capturing shock waves.

In recent years, the convective upwind and split pressure (CUSP) family schemes, which simultaneously consider the convective upwind characteristics and avoid the complex eigen-decomposition process, have achieved great success in gasdynamics. The CUSP schemes can be basically categorized to two types, the H-CUSP and E-CUSP[19, 20, 21]. The H-CUSP schemes have the total enthalpy from the energy equation in their convective vector, whereas the E-CUSP schemes use the total energy in the convective vector. The Liou's AUSM family schemes[22, 23, 24, 25, 26], Van Leer-Hänel scheme[27], and Edwards's LDFSS schemes[28, 29] belong to the H-CUSP group. The schemes developed by Zha et al.[30, 31, 32, 33, 34] belong to the E-CUSP group.

Most of the CUSP schemes mentioned above are low diffusive. However, as discussed in [35], the low diffusion scheme combined with high-order reconstruction is more probable to yield numerical oscillations in a shock wave. Agarwal et al. [36] applied the original AUSM method with first-order spatial accuracy to one-dimensional MHD cases. Han et al. [35] developed a AUSMPW+/M-AUSMPW+ schemes combined with the MLP interpolation method to achieve the higher order accuracy for MHD equations.

In this paper, an E-CUSP scheme is developed for MHD system. This scheme avoids the complication of deriving the eigenvalues and eigenvector system when the MHD equations are incorporated. The new E-CUSP scheme is used with a high order WENO reconstruction for the magnetohydrodynamics equations. The numerical experiments demonstrate the new scheme's accuracy and robustness.

2 Numerical Method

2.1 Governing Equations

The ideal MHD equations for inviscid flow can be expressed in vector form as [37]

$$\frac{\partial \mathbf{U}}{\partial t} + \nabla \cdot \mathbf{F} = 0, \tag{1}$$

where

$$\mathbf{U} = \begin{pmatrix} \rho \\ \rho\mathbf{V} \\ \mathbf{B} \\ \rho e \end{pmatrix}, \quad \mathbf{F} = \begin{pmatrix} \rho\mathbf{V} \\ \rho\mathbf{V}\mathbf{V} + p_t\mathbf{I} - \mathbf{B}\mathbf{B} \\ \mathbf{V}\mathbf{B} - \mathbf{B}\mathbf{V} \\ (\rho e + p_t)\mathbf{V} - \mathbf{B}(\mathbf{V}\cdot\mathbf{B}) \end{pmatrix},$$

$$p_t = p + \frac{1}{2}B^2, \quad \rho e = \frac{1}{2}\rho\mathbf{V}^2 + \frac{1}{2}\mathbf{B}^2 + \frac{p}{(\gamma - 1)},$$

ρ is the flow density, $\mathbf{V}$ is the velocity vector, ρe is the energy, p is the pressure, $\mathbf{B}$ is the magnetic field. The initial conditions have to satisfy

$$\nabla \cdot \mathbf{B} = 0. \tag{2}$$

The exact solution of MHD equations [Eq. (1)] keeps $\nabla \cdot \mathbf{B} = 0$ indefinitely, thus the expressions proportional to $\nabla \cdot \mathbf{B}$, the rightmost terms in Eq. (1), are zero analytically. However, in multidimensional simulations numerical errors may lead to a nonzero gradient. There are several methods[3, 17, 38] to enforce $\nabla \cdot \mathbf{B} = 0$, for example, a Leray projection corrector can be implemented at the end of each time-step,

$$\Delta\phi = -\nabla \cdot \mathbf{B} \tag{3}$$

with the approximate boundary conditions. The corrected divergence-free magnetic filed, $\mathbf{B}^c$, is realized by

$$\mathbf{B}^c = \mathbf{B} + \nabla\phi \tag{4}$$

For one dimensional case, if B_x is a constant, $\nabla \cdot \mathbf{B} = 0$ is always satisfied.

The governing equations. [Eq. (1)] can be written in the Cartesian coordinate as:

$$\frac{\partial \mathbf{U}}{\partial t} + \frac{\partial \mathbf{E}}{\partial x} + \frac{\partial \mathbf{F}}{\partial y} + \frac{\partial \mathbf{G}}{\partial z} = 0 \tag{5}$$

where

$$\mathbf{U} = \begin{bmatrix} \rho \\ \rho u \\ \rho v \\ \rho w \\ \rho e \\ B_x \\ B_y \\ B_z \end{bmatrix}, \mathbf{E} = \begin{bmatrix} \rho u \\ \rho u^2 + p_t - B_x^2 \\ \rho uv - B_x B_y \\ \rho uw - B_x B_z \\ (\rho e + p_t)u - B_x(uB_x + vB_y + wB_z) \\ uB_x - uB_x \\ uB_y - vB_x \\ uB_z - wB_x \end{bmatrix},$$

$$\mathbf{F} = \begin{bmatrix} \rho v \\ \rho uv - B_y B_x \\ \rho v^2 + p_t - B_y^2 \\ \rho vw - B_y B_z \\ (\rho e + p_t)v - B_y(uB_x + vB_y + wB_z) \\ vB_x - uB_y \\ vB_y - vB_y \\ vB_z - wB_y \end{bmatrix}, \mathbf{G} = \begin{bmatrix} \rho w \\ \rho uw - B_z B_x \\ \rho vw - B_z B_y \\ \rho w^2 + p_t - B_z^2 \\ (\rho e + p_t)w - B_z(uB_x + vB_y + wB_z) \\ wB_x - uB_z \\ wB_y - vB_z \\ wB_z - wB_z \end{bmatrix}$$

At x-direction, the speed of sound is

$$c = \sqrt{\frac{\gamma p}{\rho}},$$

the Alfven speed is

$$c_a = \frac{|B_x|}{\sqrt{\rho}},$$

and the fast and slow speeds are given by

$$c_{f,s} = \sqrt{\frac{1}{2}\left[c^2 + b^2 \pm \sqrt{(c^2+b^2)^2 - 4c^2c_a^2}\right]},$$

where $b^2 = \frac{B_x^2+B_y^2+B_z^2}{\rho}$.

In the generalized computational coordinates, Eq.(5) can be written as:

$$\frac{\partial \mathbf{U}'}{\partial t} + \frac{\partial \mathbf{E}'}{\partial \xi} + \frac{\partial \mathbf{F}'}{\partial \eta} + \frac{\partial \mathbf{G}'}{\partial \zeta} = 0, \tag{6}$$

where

$$\mathbf{U}' = \frac{1}{J}\mathbf{U},$$
$$\mathbf{E}' = \frac{1}{J}(\xi_x\mathbf{E} + \xi_y\mathbf{F} + \xi_z\mathbf{G}),$$
$$\mathbf{F}' = \frac{1}{J}(\eta_x\mathbf{E} + \eta_y\mathbf{F} + \eta_z\mathbf{G}),$$
$$\mathbf{G}' = \frac{1}{J}(\zeta_x\mathbf{E} + \zeta_y\mathbf{F} + \zeta_z\mathbf{G}).$$

At ξ-direction, the eigenvalues of the Jacobian matrix $A = \frac{\partial E'}{\partial U'}$ in system (6) are

$$U - \bar{C}_f,\ U - \bar{C}_a,\ U - \bar{C}_s,\ U,\ U, U + \bar{C}_s,\ U + \bar{C}_a,\ U + \bar{C}_f,$$

where

$$U = \xi_x u + \xi_y v + \xi_z w,$$
$$\bar{C}_a = \frac{|\bar{B}_x|}{\sqrt{\rho}},$$
$$\bar{C}_{f,s} = \sqrt{\xi_x^2+\xi_y^2+\xi_z^2}\sqrt{\frac{1}{2}\left[c^2 + b^2 \pm \sqrt{(c^2+b^2)^2 - 4c^2\frac{\bar{C}_a^2}{\xi_x^2+\xi_y^2+\xi_z^2}}\right]},$$

where $\bar{B}_x = \xi_x B_x + \xi_y B_y + \xi_z B_z$, and b^2 and c are same as in the Cartesian system. $C = c\sqrt{\xi_x^2+\xi_y^2+\xi_z^2}$ will be used in the next section.

2.2 E-CUSP scheme for MHD equations

The semi-discretized conservative one-dimensional MHD equations can be written as

$$\frac{d\mathbf{U}'}{dt} + \frac{1}{\Delta x}\left(\mathbf{E}'_{i+1/2} - \mathbf{E}'_{i-1/2}\right) = 0. \tag{7}$$

Following the E-CUSP scheme in[34], the flux $\mathbf{E}'$ may be decomposed to convective and wave flux as the following,

$$\mathbf{E}' = \mathbf{f}U + \mathbf{P} + \psi U, \tag{8}$$

where

$$
\mathbf{f} = \begin{Bmatrix} \rho \\ \rho u \\ \rho v \\ \rho w \\ \rho e \\ B_x \\ B_y \\ B_z \end{Bmatrix}, \mathbf{P} = \begin{Bmatrix} 0 \\ \xi_x p_t - B_x \bar{B}_x \\ \xi_y p_t - B_y \bar{B}_x \\ \xi_z p_t - B_z \bar{B}_x \\ -\bar{B}_x (wB_x + vB_y + wB_z) \\ -u\bar{B}_x \\ -v\bar{B}_x \\ -w\bar{B}_x \end{Bmatrix}, \psi = \begin{Bmatrix} 0 \\ 0 \\ 0 \\ 0 \\ p_t \\ 0 \\ 0 \\ 0 \end{Bmatrix}.
$$

Similar to the pressure term pU that is separated from the enthalpy term ρHU in the E-CUSP scheme, the term $p_t U$ (ψ) is also separated.

The numerical flux of the E-CUSP scheme is constructed based on the one given in[34] as the following,

$$
\mathbf{E'}_{1/2} = a_{1/2} \left[C^+ \mathbf{f}_L + C^- \mathbf{f}_R \right] + \left[D_L^+ \mathbf{P}_L + D_R^- \mathbf{P}_R \right] + \psi_{1/2}, \tag{9}
$$

where

$$
\begin{aligned}
&M_{L,R} = \frac{U_{L,R}}{a_{1/2}}, \\
&C^+ = \alpha_L^+ (1+\beta_L) M_L - \frac{1}{4}\beta_L (M_L+1)^2, \\
&C^- = \alpha_R^- (1+\beta_R) M_R + \frac{1}{4}\beta_R (M_R-1)^2, \\
&\alpha_{L,R}^{\pm} = \frac{1}{2}\left[1 \pm sign(M_{L,R})\right], \\
&\beta_{L,R} = -max\left[0, 1 - int(|M_{L,R}|)\right], \\
&D_{L,R}^{\pm} = \alpha_{L,R}^{\pm}(1+\beta_{L,R}) - \frac{1}{2}\beta_{L,R}\left(1 \pm M_{L,R}\right),
\end{aligned} \tag{10}
$$

and

$$
\psi_{1/2} = a_{1/2}(C^+ + C^-)(D^+ \phi_L + D^- \phi_R). \tag{11}
$$

Note that, in [35], the speed of a fast magnetosonic wave is used to define the Mach number $M = \frac{u}{c_f}$, which means $M_{L,R}$ is defined as $M_{L,R} = \frac{U_{L,R}}{C_{f\,1/2}}$. In the present study, we find that using $M_{L,R} = \frac{U_{L,R}}{C_f + C_{1/2}}$ is smoother and more accurate for the compound wave of Brio-Wu's shock tube, and there is almost no difference in other regions. Hence, the Mach number is defined as

$$
M_{L,R} = \frac{U_{L,R}}{a_{1/2}}, \tag{12}
$$

where

$$
a_{1/2} = \frac{1}{2}(C_{f\,L} + C_L + C_{f\,R} + C_R)
$$

is adopted.

2.3 High order WENO reconstruction[39]

The WENO scheme is used to evaluate the conservative variables U^L and U^R. The WENO scheme for a variable u^L can be written as:

$$
u_{i+1/2}^L = \sum_{k=0}^{r} \omega_k q_k, \tag{13}
$$

where $\omega_k (k = 0, \cdots, r)$ are the weights, and the $q_k (k = 0, \cdots, r)$ are the rth order accuracy reconstruction of the variables in three different stencils.

$$\omega_k = \frac{\alpha_k}{\alpha_0 + \cdots + \alpha_{r-1}}, \tag{14}$$

where

$$\alpha_k = \frac{C_k}{(\varepsilon + IS_k)^p}, \quad k = 0, 1, 2 \tag{15}$$

and where C_k are the optimal weights with the following values.

The smoothness indicators IS_k suggested by Jiang and Shu[39] are given by

$$IS_k = \sum_{l=1}^{r-1} \Delta x^{2l-1} \int_{x_{i-\frac{1}{2}}}^{x_{i+\frac{1}{2}}} (\frac{d^l}{dx^l} \hat{q}_k(x))^2 dx. \tag{16}$$

The ε in Eq.(15) is introduced to avoid the denominator becoming zero. Jiang and Shu's numerical tests indicate that the results are not sensitive to the choice of ε as long as it is in the range of 10^{-5} to 10^{-7}. In their paper[39], ε is taken as 10^{-6}. In [40], Shen et al suggested to use an optimized ε value of 10^{-2} in the smoothness estimators to achieve optimal weight in smooth regions in order to minimize dissipation and improve convergence.

The u^R is constructed symmetrically as u^L about $i + 1/2$.

For the third-order($r = 2$) WENO scheme, there are

$$q_0 = -\frac{1}{2} u_{i-1} + \frac{3}{2} u_i, \quad q_1 = \frac{1}{2} u_i + \frac{1}{2} u_{i+1},$$

and

$$\begin{gathered} C_0 = 1/3, \quad C_1 = 2/3, \\ IS_0 = (u_i - u_{i-1})^2, \quad IS_1 = (u_{i+1} - u_i)^2. \end{gathered} \tag{17}$$

For the fifth-order($r = 3$) WENO scheme, there are

$$\begin{cases} q_0 = \frac{1}{3} u_{i-2} - \frac{7}{6} u_{i-1} + \frac{11}{6} u_i, \\ q_1 = -\frac{1}{6} u_{i-1} + \frac{5}{6} u_i + \frac{1}{3} u_{i+1}, \\ q_2 = \frac{1}{3} u_i + \frac{5}{6} u_{i+1} - \frac{1}{6} u_{i+2}, \end{cases}$$

and

$$C_0 = 0.1, \quad C_1 = 0.6, \quad C_2 = 0.3.$$

The IS_k are

$$\begin{cases} IS_0 = \frac{13}{12}(u_{i-2} - 2u_{i-1} + u_i)^2 + \frac{1}{4}(u_{i-2} - 4u_{i-1} + 3u_i)^2 \\ IS_1 = \frac{13}{12}(u_{i-1} - 2u_i + u_{i+1})^2 + \frac{1}{4}(u_{i-1} - u_{i+1})^2 \\ IS_2 = \frac{13}{12}(u_i - 2u_{i+1} + u_{i+2})^2 + \frac{1}{4}(3u_i - 4u_{i+1} + u_{i+2})^2. \end{cases} \tag{18}$$

2.4 Time Marching Runge-Kutta method

The 3rd-order TVD Runge-Kutta method developed by Shu and Osher[41] is used in this paper. To solve the equation

$$\frac{du}{dt} = L(u), \tag{19}$$

the 3rd-order TVD Runge-Kutta method is

$$\begin{cases} u^{(1)} = u^{(0)} + \Delta t L(u^{(0)}) \\ u^{(2)} = \dfrac{3}{4}u^{(0)} + \dfrac{1}{4}u^{(1)} + \dfrac{1}{4}\Delta t L(u^{(1)}) \\ u^{(3)} = \dfrac{1}{3}u^{(0)} + \dfrac{2}{3}u^{(2)} + \dfrac{2}{3}\Delta t L(u^{(2)}). \end{cases} \tag{20}$$

3 Numerical examples

3.1 One-dimensional Riemann problems

(1) Brio-Wu shock tube problem

The initial left and right values have been suggested by Brio and Wu[1] and are commonly used to test numerical schemes for one-dimensional ideal MHD. Note that the hydrodynamics data used here are identical to those in Sod's shock tube Riemann problem.

$$(\rho, u, v, w, B_y, B_z, p) = \begin{cases} (1.0, \quad 0, 0, 0, +1, 0, 1.0), & for\ x < 0 \\ (0.125, 0, 0, 0, -1, 0, 0.1), & for\ x > 0 \end{cases}$$

with $B_x = 0.75$, $\gamma = 2$.

The numerical example involves a compound wave, which is a typical feature of the solutions of MHD systems. For each quantity, the solution contains five constant states separated by a fast rarefaction wave, a slow compound wave, a slow shock, and a fast rarefaction. The density presents a sixth constant state because this variable is discontinuous across the contact discontinuity[1].

Fig. 1 shows the solution with 800 points at $t = 0.2$. It can be seen that the present method resolves well all the complex waves.

(2) High Mach number shock tube problem

In the second tested case the following initial values are used to demonstrate the robustness of the present scheme for high Mach number flow in MHD. The Mach number corresponding to the right-moving shock wave is 15.5. This problem is also used in[1, 4].

$$(\rho, u, v, w, B_y, B_z, p) = \begin{cases} (1.0, \quad 0, 0, 0, +1, 0, 1000), & for\ x < 0 \\ (0.125, 0, 0, 0, -1, 0, 0.1), & for\ x > 0 \end{cases}$$

with $B_x = 0$, $\gamma = 2$.

The numerical result with 200 points at $t = 0.012$ is shown in Fig. 2. There is a slight undershoot at the tail of the rarefaction wave. The contact discontinuity and shock wave are captured very well. These numerical results agree well with those of Jiang and Wu[4] and show that the present scheme can deal well with MHD high Mach number flow.

3.2 Two-dimensional Kelvin-Helmholtz instability

The Kelvin-Helmholtz instabilty is considered as an important mechanism for momentum transfer at Earth's magnetopause boundary, which separates the solar wind flow from the Earth's magnetoshpere[42, 4]. In order to compare the results, the computational conditions are taken as the same used in [4, 17]. The initial stationary configuration of the periodic model is given by

$$\begin{array}{l} \rho_0 = 1, \quad u = \frac{u_0}{2}\tanh(y/a), \quad v = w = 0, \\ p_0 = 0.5, \quad B_{x0} = B_{y0} = 0, \quad B_{z0} = 1, \end{array}$$

where a denotes the width of the velocity shear layer. At $t = 0$, a small perturbation of the following form is introduced,

$$\tilde{u}_0 = \begin{cases} -\bar{u}_0 \sin(2\pi x/\lambda)/(1+y^2), & if \ -\frac{\lambda}{2} < x < \frac{\lambda}{2}, \\ 0, & otherwise \end{cases}$$

The computational domain is $[-\frac{L}{2}, \frac{L}{2}] \times [0, H]$. $u_0 = 2$, $\bar{u}_0 = 0.008$, $L = \lambda = 5\pi$, $H = 1$, $a = 1$, and $\gamma = 2$ are used. The periodic boundary condition is used in the x-direction. The free outflow condition is applied at the top boundary at $y = H$. At the low boundary of y-direction, ρ, p, and B_z are symmetric and u and v are antisymmetric under the transformation $x \rightarrow -x$.

A Roberts transformation[4, 17]

$$y = \frac{H \sinh(\tau\eta/2H)}{\sinh(\tau/2)}$$

with $\tau = 6$ is used to refine the grid near $y = 0$. The mesh has 96×60 grid points. Fig. 3 shows the current computational results. In calculation, the components of B_x, B_y, and w are always zero and the evolution of B_z follows closely with that of the density. They are in excellent agreement with Jiang and Wu's results[4].

3.3 Orszag-Tang MHD turbulence problem

Since the Orszag-Tang MHD turbulence problem[43] has many significant characteristics of MHD turbulence, such as interactions of multiple shock waves generated as the vortex evolves, it is considered as one of the standard models to validate a MHD numerical method[44, 4, 45, 17, 35].

The initial conditions are given by

$$\begin{array}{lll} \rho(x,y,0) = \gamma^2, & u(x,y,0) = -\sin(y), & v(x,y,0) = \sin(x), \\ p(x,y,0) = \gamma, & B_x(x,y,0) = -\sin(y), & B_y(x,y,0) = \sin(2x), \end{array}$$

where $\gamma = 5/3$. As in [44, 4, 45], the computational domain is $[0, 2\pi] \times [0, 2\pi]$ with a uniform mesh of 192×192 grid points. Periodic boundary conditions are imposed in both x- and y-directions. Figs. 4-6 show the numerical results at times $t = 0.5$, 2, and 3, where 20 contours are plotted. The current results are very close to Jiang and Wu's[4] numerical solutions.

4 Conclusions

An E-CUSP scheme that avoids the complex eigenstructure of the Jacobian matrices in MHD system, is developed and used with a fifth order WENO scheme to solve 1D and 2D MHD problems. The numercal testing shows that the scheme can resolve the complex wave characteristics in MHD very well.

5 Acknowledgment

This work was supported in part by the U. S. Air Force Office of Scientific Research under Grants FA9550-09-1-0105 monitored by Dr. Robert Barker.

References

[1] M. Brio, C. C. Wu, "An upwind differencing scheme for the equations of ideal magnetohydrodynamics," *Journal of Computational Physics*, vol. 75, pp. 400–422, 1988.

[2] P. L. Roe, D. S. Balsara, "Notes on the eigensystem of magnetohydrodynamics," *SIAM J. Appl. Math.*, vol. 56, pp. 57–67, 1996.

[3] K. G. Powell, P. L. Roe, T. J. Linde, T. I. Gombosi, D. L. De Zeeuw, "A Solution-Adaptive Upwind Scheme for Ideal Magnetohydrodynamics," *Journal of Computational Physics*, vol. 154, pp. 284–309, 1999.

[4] Guang-Shan Jiang, Cheng-chin Wu, "A High-Order WENO Finite Difference Scheme for the Equations of Ideal Magnetohydrodynamics," *Journal of Computational Physics*, vol. 150, pp. 561–594, 1999.

[5] K. Murawski, *Analytical and numerical methods for wave propagation in fluid media.* World Scientific Publising Co., 2002.

[6] W.L. Dai, P. R. Woodward, "An Approximate Riemann Solver for Ideal Magnetohydrodynamics," *Journal of Computational Physics*, vol. 111, pp. 354–372, 1994.

[7] A. L. Zachary, P. Colellaz, "A higher-order godunov method for the equations of ideal magnetohydrodynamics," *Journal of Computational Physics*, vol. 99, pp. 341–347, 1992.

[8] P. Cargo, G. Gallice, "Roe Matrices for Ideal MHD and Systematic Construction of Roe Matrices for Systems of Conservation Laws," *Journal of Computational Physics*, vol. 136, pp. 446–466, 1997.

[9] P. Janhunen, "A Positive Conservative Method for Magnetohydrodynamics Based on HLL and Roe Methods," *Journal of Computational Physics*, vol. 160, pp. 649–661, 2000.

[10] V. Honkkila, P. Janhunen, "HLLC solver for ideal relativistic MHD," *Journal of Computational Physics*, vol. 223, pp. 643–656, 2007.

[11] K. F. Gurski, "An HLLC-type approximate Riemann solver for ideal magnetohydrodynamics," *SIAM J. Sci. Comp.*, vol. 25, pp. 2165–2187, 2004.

[12] S. T. Li, "An HLLC Riemann solver for magneto-hydrodynamics," *Journal of Computational Physics*, vol. 203, pp. 344–357, 2005.

[13] T. Miyoshi, K. Kusano, "A multi-state HLL approximate Riemann solver for ideal magnetohydrodynamics," *Journal of Computational Physics*, vol. 208, pp. 315–344, 2005.

[14] Dinshaw S. Balsara, Tobias Rumpf, Michael Dumbser, Claus-Dieter Munz, "Efficient, high accuracy ADER-WENO schemes for hydrodynamics and divergence-free magnetohydrodynamics," *Journal of Computational Physics*, vol. 228, pp. 2480–2516, 2009.

[15] R. W. MacCormack, "An upwind conservation form method for ideal magnetohydrodynamics equations." AIAA Paper 99-3609, 1999.

[16] H.C. Yee, B. Sjogreen, "Development of low dissipative high order filter schemes for multiscale Navier-Stokes/MHD systems," *Journal of Computational Physics*, vol. 225, pp. 910–934, 2007.

[17] J. Balbas, E. Tadmor, C.-C. Wu, " Non-oscillatory central schemes for one- and two-dimensional MHD equations: I," *Journal of Computational Physics*, vol. 201, pp. 261–285, 2004.

[18] D. V. Gaitonde, "Development of a solver for 3-D non-ideal magnetogasdynamics." AIAA Paper 99-3610, 1999.

[19] A. Jameson, "Analysis and Design of Numerical Schemes for Gas Dynamics I: Artificial Diffusion, Upwind Biasing, Limiters and Their Effect on Accuracy and Multigrid Convergence in Transonic and Hypersonic Flow." AIAA Paper 93-3359, July, 1993.

[20] A. Jameson, "Analysis and Design of Numerical Schemes for Gas Dynamics I: Artificial Diffusion, Upwind Biasing, Limiters and Their Effect on Accuracy and Multigrid Convergence in Transonic and Hypersonic Flow," *Journal of Computational Fluid Dynamics*, vol. 4, pp. 171–218, 1995.

[21] A. Jameson, "Analysis and Design of Numerical Schemes for Gas Dynamics II: Artificial Diffusion and Discrete Shock Structure," *Journal of Computational Fluid Dynamics*, vol. 5, pp. 1–38, 1995.

[22] M.-S. Liou and C. J. Steffen, "A New Flux Splitting Scheme," *Journal of Computational Physics*, vol. 107, pp. 1–23, 1993.

[23] Y. Wada and M.-S. Liou, "An Accurate and Robust Splitting Scheme for Shock and Contact Discontinuities." AIAA Paper 94-0083, 1994.

[24] M.-S. Liou, "Progress Towards an Improved CFD Methods: AUSM$^+$." AIAA Paper 95-1701-CP, June, 1995.

[25] M.-S. Liou, "A Sequel to AUSM: AUSM$^+$," *Journal of Computational Physics*, vol. 129, pp. 364–382, 1996.

[26] M.-S. Liou, "Ten Years in the Making-AUSM-Family." AIAA 2001-2521, 2001.

[27] D. Hänel, R. Schwane, G. Seider, "On the Accuracy of Upwind Schemes for the Solution of the Navier-Stokes Eqautions." AIAA paper 87-1105 CP, 1987.

[28] J. R. Edwards, "A Low-Diffusion Flux-Splitting Scheme for Navier-Stokes Calculations." AIAA Paper 95-1703-CP, June, 1995.

[29] J. R. Edwards, "A Low-Diffusion Flux-Splitting Scheme for Navier-Stokes Calculations," *Computer & Fluids*, vol. 6, pp. 635–659, 1997.

[30] G. -C. Zha, E. Bilgen, "Numerical Solutions of Euler Equations by Using a New Flux Vector Splitting Scheme ," *International Journal for Numerical Methods in Fluids*, vol. 17, pp. 115–144, 1993.

[31] G.-C. Zha, "Numerical Tests of Upwind Scheme Performance for Entropy Condition ," *AIAA Journal*, vol. 37, pp. 1005–1007, 1999.

[32] G.-C. Zha, "Comparative Study of Upwind Scheme Performance for Entropy Condition and Discontinuities." AIAA Paper 99-CP-3348, June 28- July 1, 1999.

[33] G.-C. Zha and Z.-J. Hu, "Calculation of Transonic Internal Flows Using an Efficient High Resolution Upwind Scheme," *AIAA Journal*, vol. 42, No. 2, pp. 205–214, 2004.

[34] G.-C. Zha, Y.-Q. Shen, B.-Y. Wang, "Calculation of Transonic Flows Using WENO Method with a Low Diffusion E-CUSP Upwind Scheme." AIAA Paper 2008-0745, Jan 2008.

[35] Sang-Hoon Han, Jeong-Il Lee, Kyu Hong Kim, " Accurate and Robust Pressure Weight Advection Upstream Splitting Method for Magnetohydrodynamics Equations," *AIAA Journal*, vol. 47, pp. 970–981, 2009.

[36] R. K. Agarwal, J. Augustinus, and D. W. Halt, "A Comparative Study of Advection Upwind Split (AUSM) and Wave/Particle Split (WPS) Schemes for Fluid and MHD Flows." AIAA-1999-3613, 1999.

[37] H.-M. Damevin, K. A. Hoffmann, "Development of a modified Runge-Kutta scheme with TVD limiters for ideal three-dimensional magnetogasdynamics." AIAA 2001-2739, 2001.

[38] J. U. Brackbill, D. C. Barnes, "The Effect of Nonzero backward difference $\nabla \cdot B$ on the numerical solution of the magnetohydrodynamic equations," *Journal of Computational Physics*, vol. 35, pp. 426–430, 1980.

[39] G.-S. Jiang, C.-W. Shu, "Efficient implementation of weighted ENO schemes," *J.Comput.Phys.*, vol. 126, pp. 202–228, 1996.

[40] Y.-Q. Shen, G.-C. Zha, B.-Y. Wang, "Improvement of stability and accuracy of implicit WENO scheme," *AIAA Journal*, vol. 47, pp. 331–344, 2009.

[41] C.-W. Shu, O. Osher, "Efficient implementation of essentially non-oscillatory shock capturing schemes," *Journal of Computational Physics*, vol. 77, pp. 439–471, 1988.

[42] C. C. Wu, "Kelvin-Helmholtz instability at the magnetopause boundary," *Journal of Geophysical Research*, vol. 91, pp. 3042–3060, 1986.

[43] S. A. Orszag, C. M. Tang, " Small-scale structure of two-dimensional magnetohydrodynamic turbulence," *J. Fluid. Mech.*, vol. 90, pp. 129–143, 1979.

[44] A. Zachary, A. Malagoli, and P. Colella, "A high-order Godunov method for multidimensional ideal magnetohydrodynamics," *SIAM J. Sci. Comput.*, vol. 15, pp. 263–284, 1994.

[45] H. Z. Tang, K. Xu, "A high-order gas-kinetic method for multidimensional ideal magnetohydrodynamics," *Journal of Computational Physics*, vol. 165, pp. 69–88, 2000.

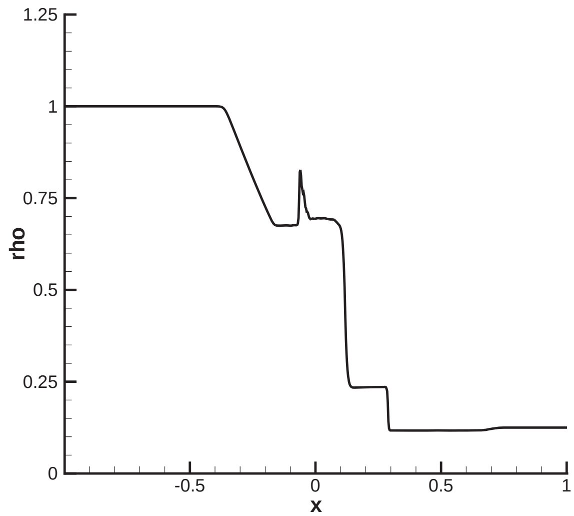

Density

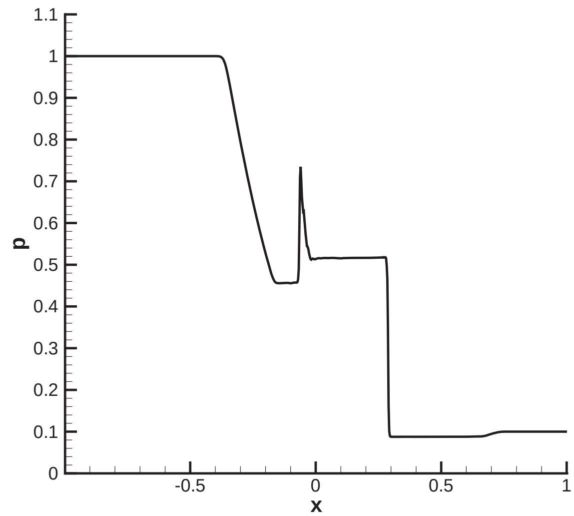

Pressure

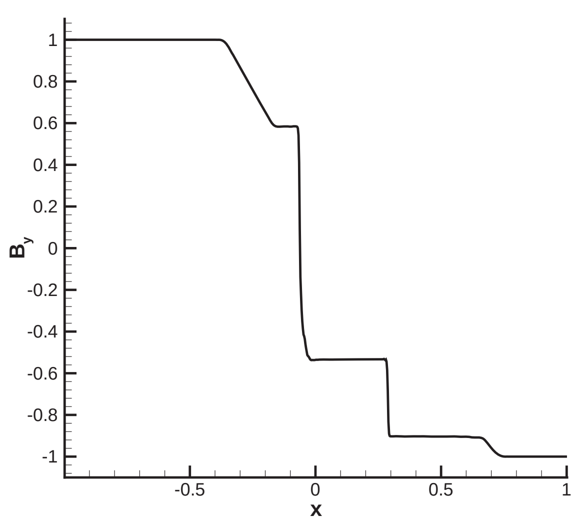

B_y

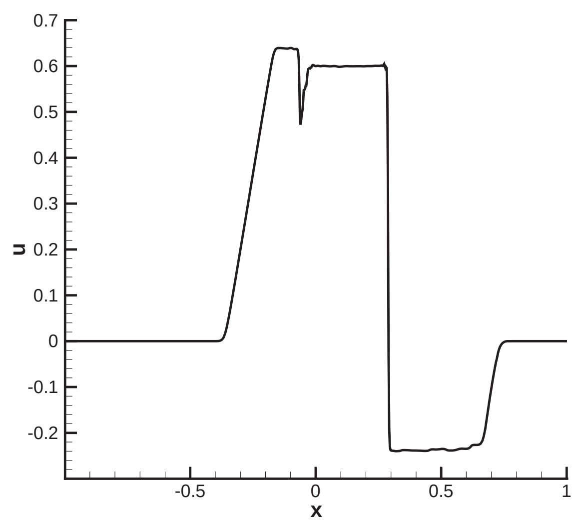

Velocity, u

Figure 1: Brio-Wu shock tube problem

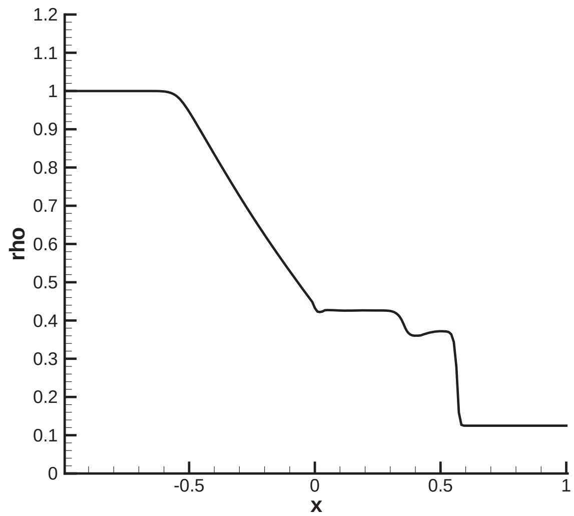

Density

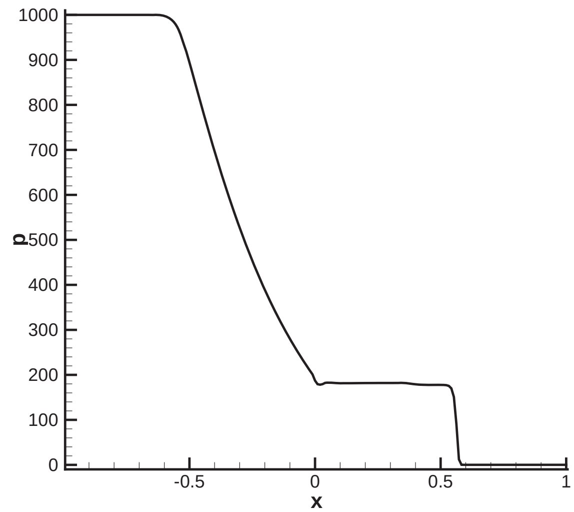

Pressure

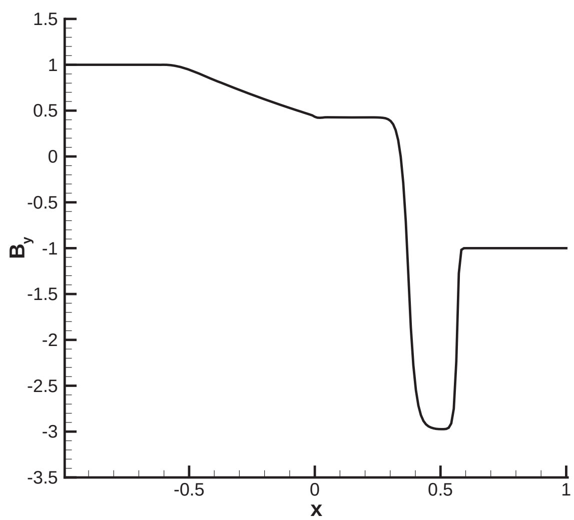

B_y

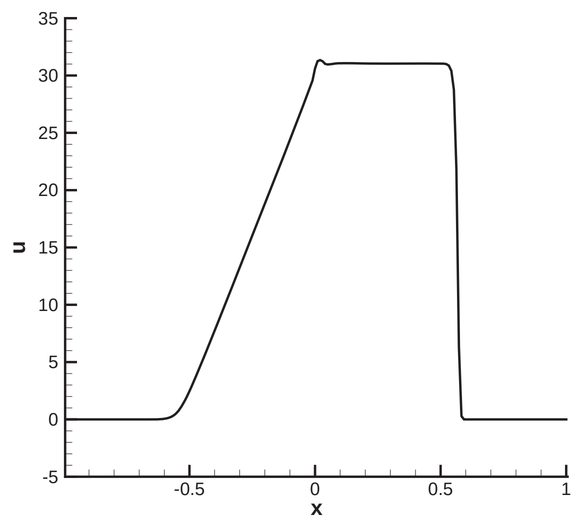

Velocity, u

Figure 2: High Mach number shock tube problem

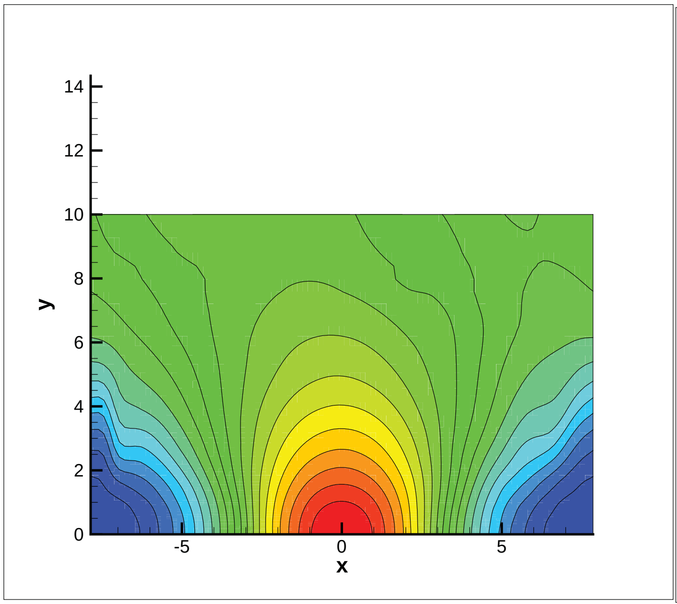

Density contours

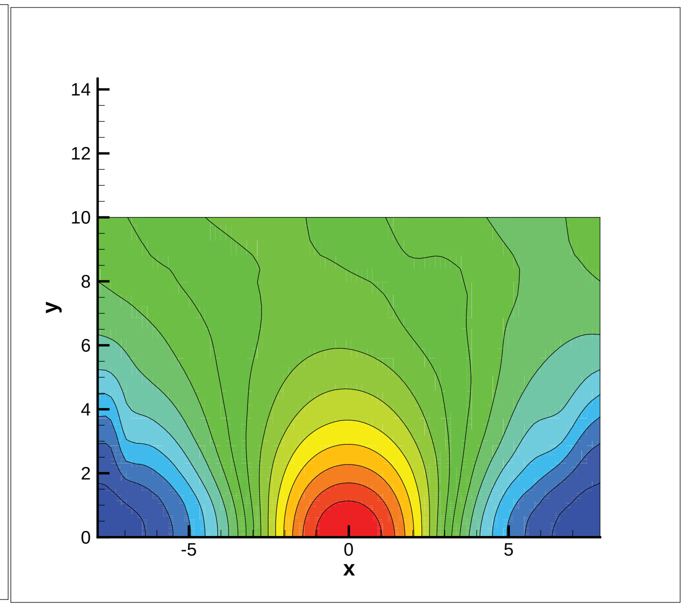

Pressure contours

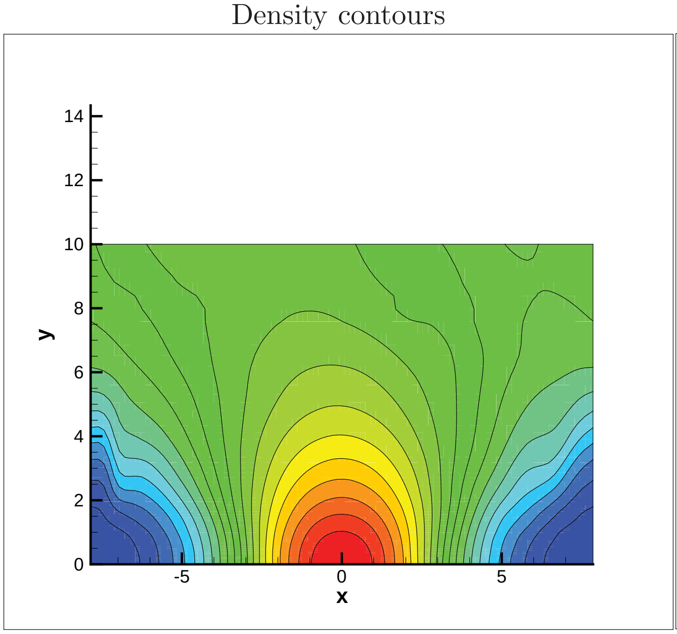

B_z contours

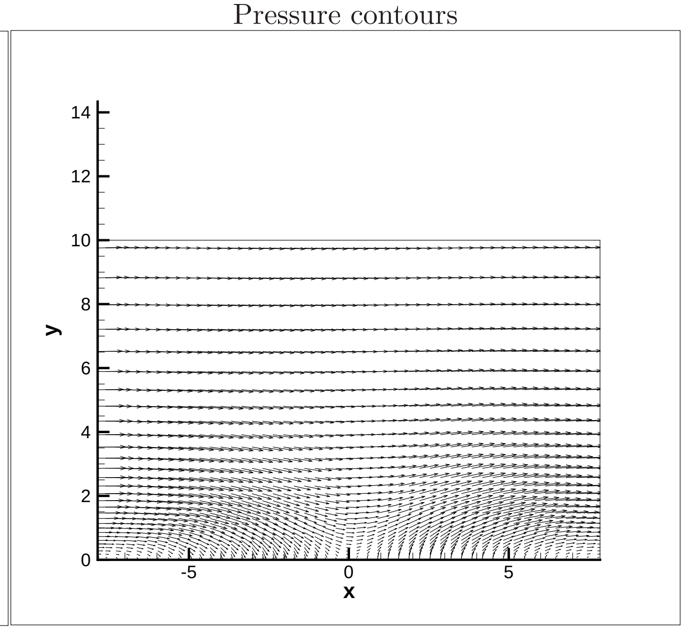

Velocity fields

Figure 3: Two-dimensional Kelvin-Helmholtz instability

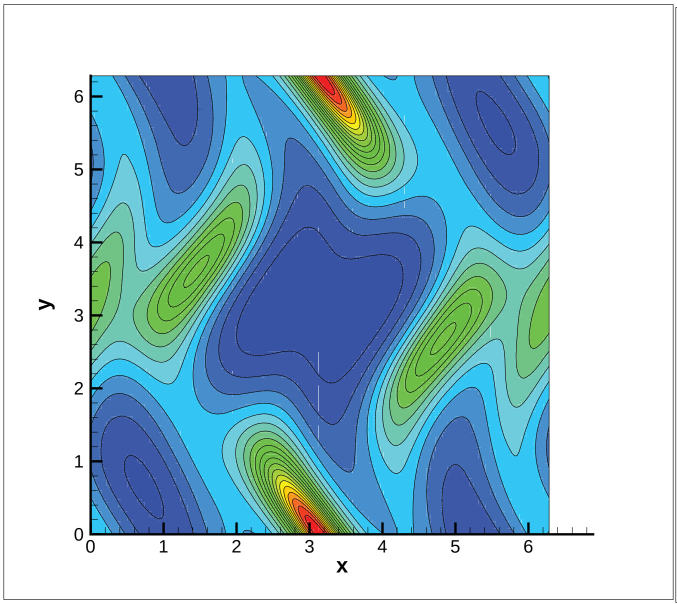

Density contours

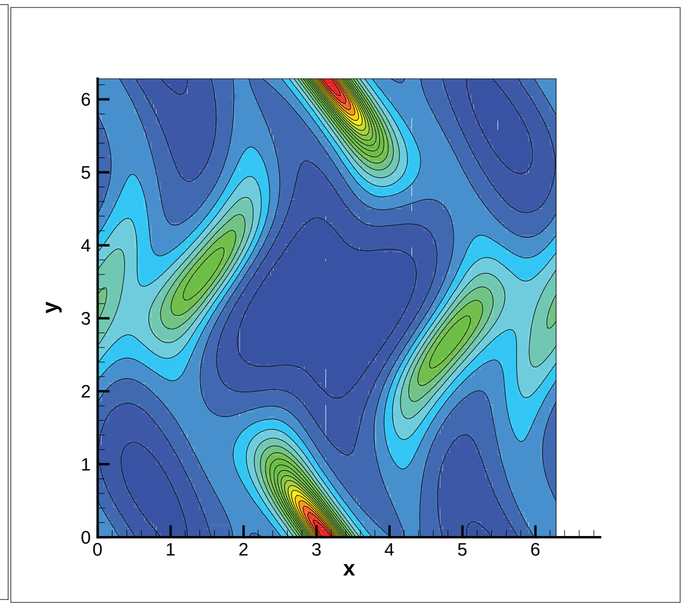

Pressure contours

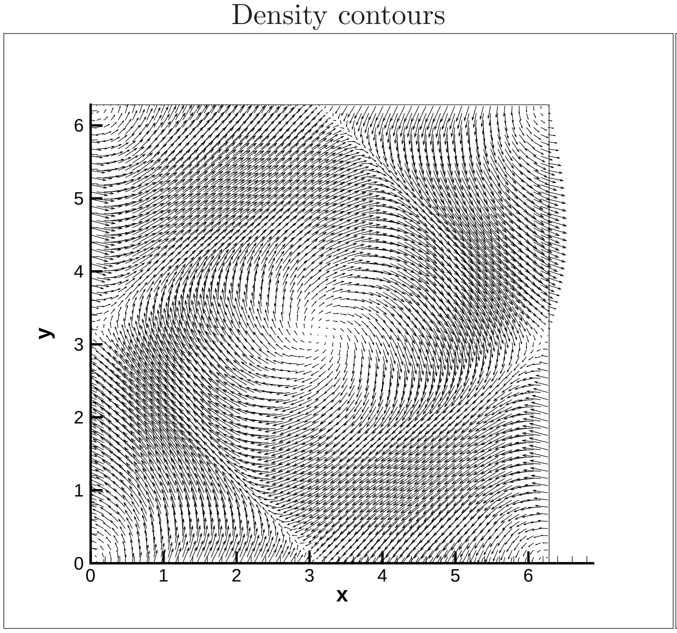

Velocity fields

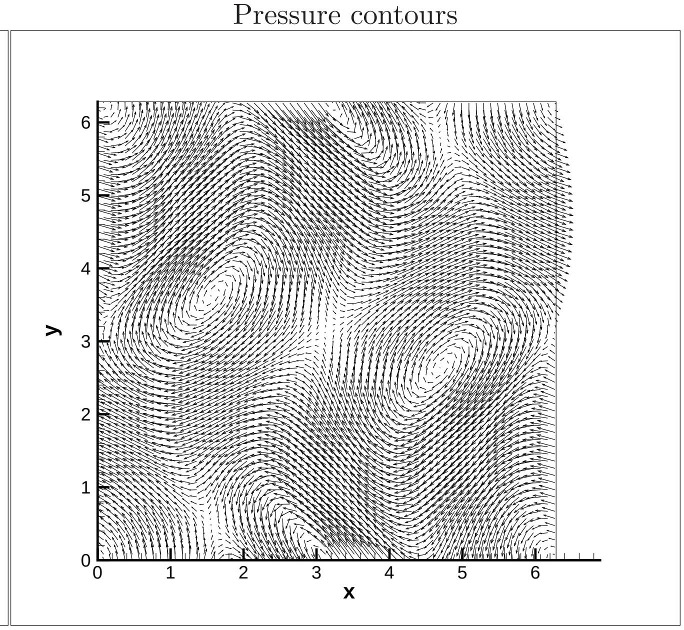

Magnetic fields

Figure 4: Orszag-Tang MHD turbulence problem, $t = 0.5$

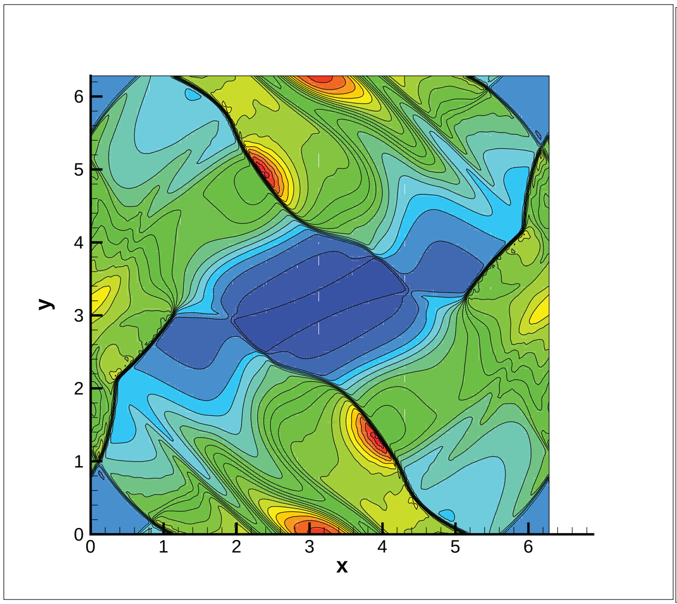

Density contours

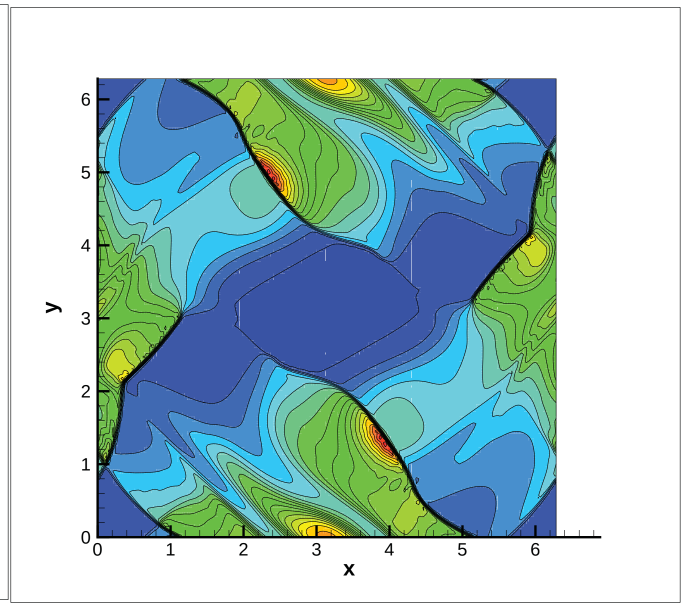

Pressure contours

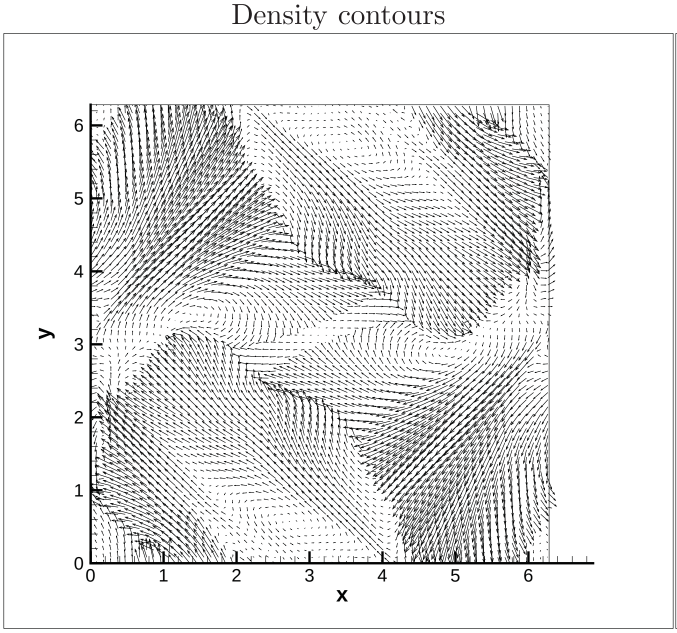

Velocity fields

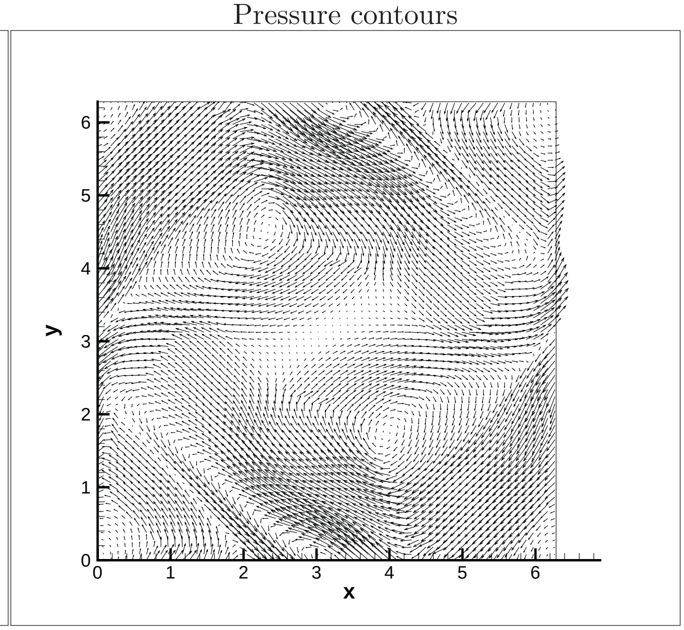

Magnetic fields

Figure 5: Orszag-Tang MHD turbulence problem, $t = 2.0$

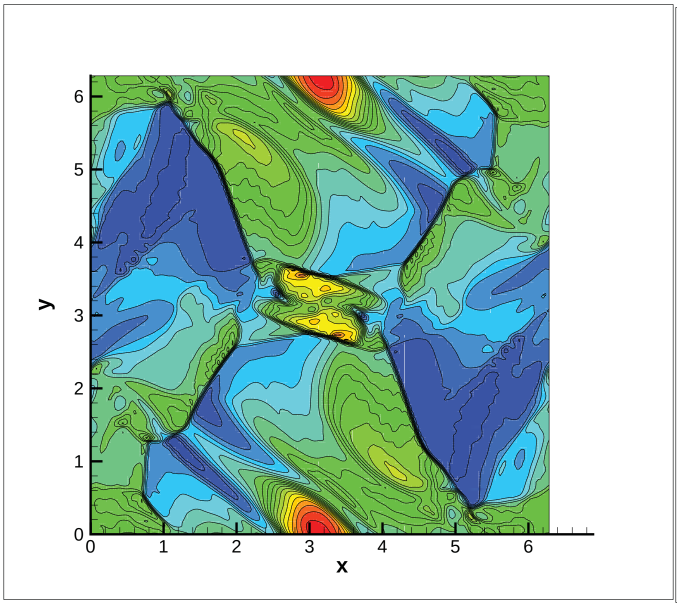

Density contours

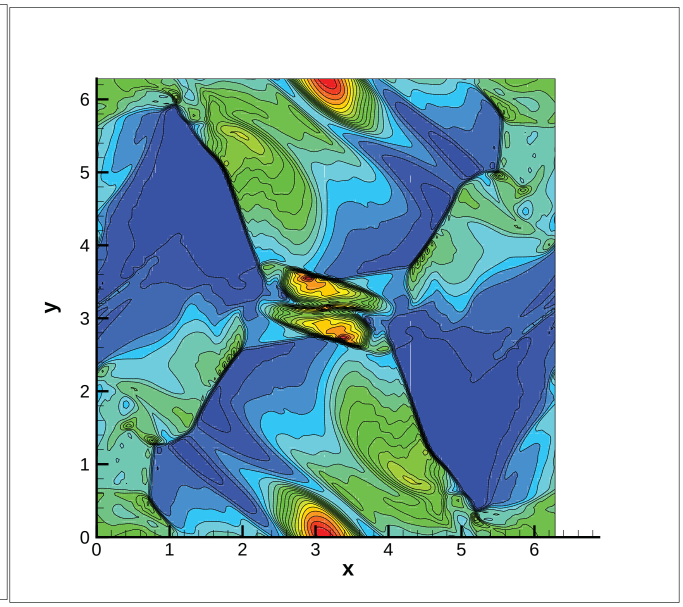

Pressure contours

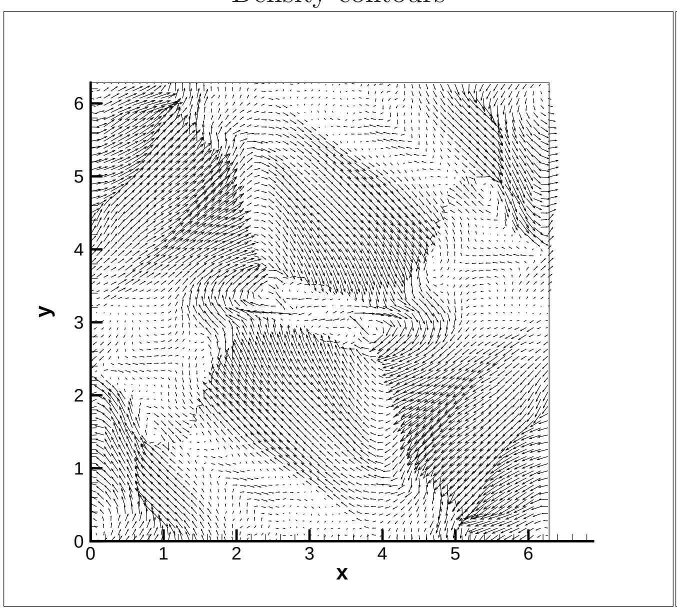

Velocity fields

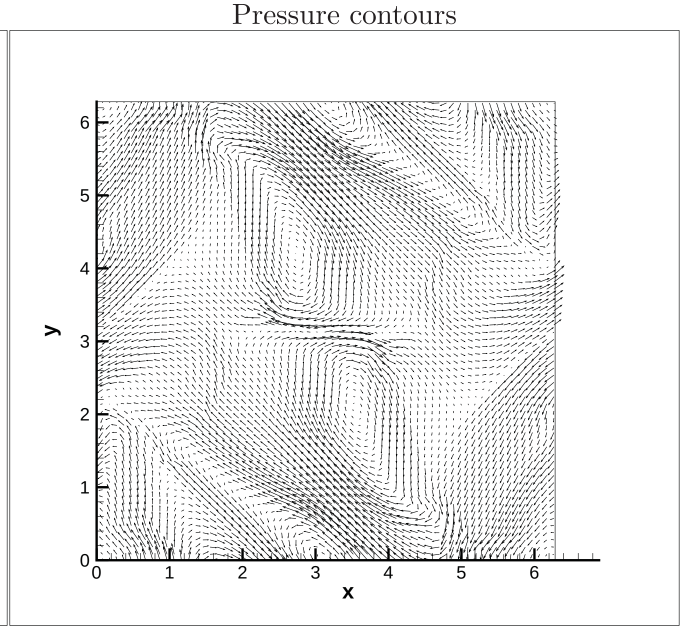

Magnetic fields

Figure 6: Orszag-Tang MHD turbulence problem, $t = 3.0$